Molecular Ecology (2008) **17**, 1718–1731 doi: 10.1111/j.1365-294X.2008.03609.x

Directional dispersal between mid-ocean ridges: deep-ocean circulation and gene flow in *Ridgeia piscesae*

C. R. YOUNG,*† S. FUJIO‡ and R. C. VRIJENHOEK*

**Monterey Bay Aquarium Research Institute, 7700 Sandholdt Road, Moss Landing, CA 95039-9644, USA, †Department of Ecology and Evolutionary Biology, University of California, Santa Cruz, 1156 High Street, Santa Cruz, CA 95064, USA, ‡Ocean Research Institute, University of Tokyo, 1-15-1, Minamidai, Nakano-ku, Tokyo 164-8639, Japan*

Abstract

This study examined relationships between bathymetrically induced deep-ocean currents and the dispersal of the hydrothermal vent tubeworm *Ridgeia piscesae* along the northeast Pacific ridge system. A robust diagnostic model of deep-ocean circulation in this region predicted strong southeasterly currents following contours of the Blanco Transform Fault, a 450-km lateral offset that separates the Gorda and Juan de Fuca ridge systems. Such currents should facilitate the southward dispersal of *R. piscesae* larvae. Immigration rates for populations north and south of the Blanco Transform Fault were estimated from molecular population genetic data. Mitochondrial DNA evidence revealed population subdivision across the Blanco Transform Fault, and a strong directional bias in gene flow that was consistent with predictions of the circulation model. The distribution of mitochondrial diversity between the northern and southern populations of *R. piscesae* suggests that the Gorda Ridge tubeworms have maintained larger effective population sizes than the northern populations, a pattern that also exists in co-occurring limpets. Together, these data suggest that the northern vent fields may experience a higher frequency of habitat turnover and consequently more rapid losses of genetic diversity.

Keywords: coalescent, deep ocean circulation, gene flow, hydrothermal vent, model adequacy, *Ridgeia piscesae*

Received 4 November 2006; revision received 7 July 2007; accepted 20 October 2007

Introduction

Historically, the deep-sea benthos was considered a temporally and spatially homogeneous environment (reviewed by Gage & Tyler 1991). The vast majority of animals occupying this realm disperse as larvae that are transported by strong oceanic currents; thus, limited opportunities for isolation of populations and speciation were believed to exist (Palumbi 1994). Recent molecular studies challenge this notion, however, and many marine taxa that were previously identified as cosmopolitan species are now known to exhibit significant population subdivision and cryptic speciation on geographical (horizontal) and bathymetrical (vertical) scales (Etter & Rex 1990; France & Kocher 1996; Etter *et al*. 1999; Barber *et al*. 2000).

Deep-sea hydrothermal vent animals provide notable exceptions to the benthic uniformity argument (reviewed in Vrijenhoek 1997; recent examples in Goffredi *et al*. 2003; Won *et al*. 2003; Hurtado *et al*. 2004; Johnson *et al*. 2006). Vent communities are scattered along the global mid-ocean ridge system and are associated with isolated submarine volcanoes and back-arc basins. Vent food webs are based on chemoautotrophic microbes that metabolize reduced compounds (primarily CH_4 and H_2S) dissolved in hydrothermal effluents, and the microbes are eaten directly or used as symbionts by diverse invertebrate animals (Cavanaugh 1994; Bright & Giere 2005). Dependence of vent communities on these transient gases leads to frequent local extinction and recolonization events (Haymon *et al*. 1993; Shank *et al*. 1998). To persist, vent-endemic species must be capable of dispersing effectively between fields and colonizing nascent habitats when they arise (Vrijenhoek

Correspondence: C. R. Young, Department of Organismic and Evolutionary Biology, Harvard University, 16 Divinity Avenue, Cambridge, MA 02138, USA. Fax: 617-496-6933; E-mail: cyoung@oeb.harvard.edu

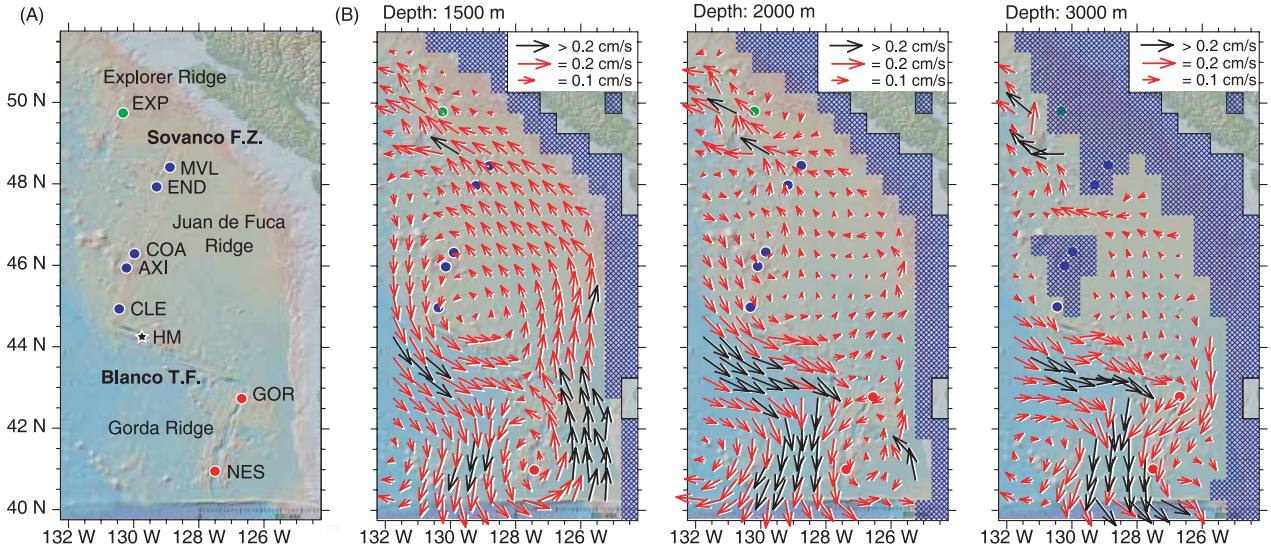

Fig. 1 (a) Bathymetric map of sampling locations. Colours denote the by-ridge pooling scheme used in the analyses of variance: green, Explorer Ridge; blue, Juan de Fuca Ridge; red, Gorda Ridge. The location of a hydrothermal mound and helium anomalies in the water column is labelled HM. (b) Current vectors calculated from the circulation model for three depths: 1500, 2000 and 3000 m.

1997). Hydrothermal plume-induced circulation appears to transport larvae along corridors constrained by walls that flank the axial valleys of many ridge systems (Mullineaux *et al*. 1991; Mullineaux & France 1995; Kim & Mullineaux 1998; Thomson *et al*. 2003; Mullineaux *et al*. 2005). Occasional megaplume events are hypothesized to transport larvae across longer distances and between disjunct ridge systems (Kim *et al*. 1994). Dispersal outside or above the rift valleys might expose dispersing larvae to cross-axis currents that carry them off-axis and remove them from the larval supply. Benthic features such as lateral offsets in a ridge system (i.e. transform faults), intervening seamounts and microplates, and abrupt changes in bathymetry are associated with shifts in deep-ocean circulation (Warren 1981; Reid 1986; Fujio & Imasato 1991; Reid 1997; Thomson *et al*. 2003; Thurnherr & Speer 2003). Hence, strong cross-axis currents could disrupt along-axis gene flow and contribute to isolation and speciation for a number of vent-endemic animals (O'Mullan *et al*. 2001; Won *et al*. 2003; Hurtado *et al*. 2004).

The goals of this study were to assess whether deep-ocean circulation patterns affect genetic diversity and dispersal rates among *Ridgeia piscesae* (Polychaeta: Siboglinidae) tubeworm populations from hydrothermal vent fields along the northeastern Pacific ridge systems (Fig. 1a). This study was stimulated by a recent discovery that closely related sister species of vent limpets, *Lepetodrilus fucensis* and *L. gordensis*, are separated by the Blanco Transform Fault, a 450-km long lateral offset that separates the Gorda and Juan de Fuca ridges (Johnson *et al*. 2006). Essentially, no genetic subdivision exists among conspecific subpopulations of either species living north and south of this barrier. The two species appear to be isolated now, but if limited interspecific gene flow exists or has occurred in the recent past, it flowed in a southeasterly direction and not the reverse. For these limpets, the northeastern ridge systems can be partitioned into two dispersal corridors: (i) a northern corridor that crosses the Sovanco Fracture Zone and encompasses the Juan de Fuca and Explorer ridges; and (ii) a southern corridor composed of Gorda Ridge populations. The southern limpets retain significantly more genetic diversity than the northern populations. Thus, it was hypothesized that the northern vent fields may be more ephemeral than southern vent fields along the Gorda Ridge (Johnson *et al*. 2006). The present study aims to examine these hypotheses by examining *R. piscesae* samples from the same range. To assess the potential effects of ocean currents on the dispersal of these worms, we generated a model of deep-ocean circulation for this region, parameterized by temperature and salinity data. Genetic data from mitochondrial cytochrome *c* oxydase subunit I (COI) sequences and multilocus allozyme data were used to assess genetic diversity, population subdivision and gene flow in *R. piscesae*. If current vectors and habitat stability similarly effect neutral genetic variation in these animals, we expect patterns of diversity in the tubeworms to generally mirror those in the limpets. Nevertheless, the magnitude of these effects may vary because of demographic and larval life-history differences between these animals (e.g. Hurtado *et al*. 2004).

Table 1 Northwestern Pacific hydrothermal vent localities. Locations are in decimal degrees and depth is in metres

							Sample size	
Vent field	Abbr.	N latitude	W longitude	Dive*	Date	Depth	Allozymes	COI
S. Explorer Ridge	EXP	49.760	130.259	A2807	7/28/1994	1814	18	24
Middle Valley	MVL	48.457	128.709	A2803	7/24/1994	2416	10	20
		48.454	128.711	A2805	7/26/1994	2417	12	15
Endeavor segment	END	47.970	129.087	A2425	8/09/1991	2180	20	20
Co-Axial	COA	46.301	129.710	A2793	7/07/1994	2268	9	9
Axial Volcano	AXI	45.935	130.013	A2426	8/10/1991	1547	20	10
		45.933	129.981	T182	7/28/2000	1519	20	9
Cleft segment	CLE	44.655	130.367	A2427	8/11/1991	2227	—	10
		44.658	130.363	T180	7/26/2000	2202	10	8
		44.990	130.201	T184	7/30/2000	2238	10	11
Gorda Ridge	GOR	42.755	126.703	A2799	7/19/1994	2847	6	10
		42.754	126.709	T188	8/08/2000	2700	8	—
		42.754	126.709	T454	7/28/2002	2695	15	—
		42.754	126.711	T456	7/30/2002	2745	20	16
N. Escanaba Trough	NES	41.007	127.488	A2036	6/06/1988	3240	10	8
		41.001	127.492	A2800	7/20/1994	3317	—	10
		41.000	127.493	T449-1	7/23/2002	3220	11	18
		41.001	127.493	T449-3	7/23/2002	3220	10	18

*Dive numbers are labelled A, Alvin; T, Tiburon.

Methods

Circulation model

Circulation patterns in the study region were estimated with the robust diagnostic model of Fujio & Imasato (1991). Details of the model are published elsewhere (Fujio & Imasato 1991). Estimates of ocean currents are generated from hydrostatic pressure, as determined from water density and wind stress. Water density is estimated from temperature and salinity (World Ocean Atlas 1994; published by the National Oceanographic Data Center), which were used to parameterize the model. Estimated circulation vectors are insensitive to the data set used to parameterize the model (World Ocean Atlas 1982; sensitivity analysis, data not shown).

The horizontal resolution was increased from two-degree grids as set in the earlier model (Fujio & Imasato 1991) to half-degree grids in the present model. The vertical resolution (depth) was composed of 29 levels. The time domain of the model was 24 years. A latitude-dependent restoration term was used with a restoration term of 200 days for mid-latitudes. Circulation reached a steady state within this time horizon. Deep circulation is controlled by bottom topography, and the half-degree grid of the model is not sufficiently fine to resolve seamounts, ridges and trenches. Therefore, the model is not expected to accurately reproduce fine-scale circulation patterns induced by ridge topography. The weak velocity of the model was also related to the resolution. The model computes the fluid transport (cross-section × velocity), not the velocity. Currents that are narrower than the model grid are widened by viscosity in the model, and current velocity is weakened as a reciprocal of current width. Because of this relationship, transport is not affected by model resolution. We report current vectors (Fig. 1b) at three depths roughly corresponding to the depths of our sampling locations (1500, 2000 and 3000 m).

Samples and genetic methods

Specimens were collected with manned and unmanned submersibles during oceanographic expeditions that spanned from 1988 to 2003 (Fig. 1a, Table 1). Whole specimens were frozen at –80 °C, and samples were transported on dry ice to the land-based laboratory and stored at –80 °C. Tissue samples for allozyme studies were homogenized in an equal volume of grinding buffer (0.01 M Tris, 2.5 mM EDTA, pH 7.0) and centrifuged at 8000× g for 2 min to remove cellular debris. Cellulose acetate gel electrophoresis (CAGE) was used to screen eight allozyme loci that were previously shown to be polymorphic in *Ridgeia piscesae* (Southward *et al*. 1995). We report on only four of these loci (Aat-1, Idh, Mdh-1, and Mpi) that could be resolved with the CAGE method. Electrophoretic conditions, buffers and stains followed standard methodology (Hebert & Beaton 1989).

Genomic DNA was isolated using the QIAGEN DNeasy DNA extraction kit (QIAGEN Inc.). A 710-bp fragment of

mitochondrial COI was amplified with universal invertebrate primers (Folmer *et al*. 1994): initial denaturation of 95 °C/5 min, followed by 35 cycles of 94 °C/1 min, 45 °C/1 min, and 72 °C/2 min, and a final extension at 72 °C/7 min. Amplicons were gel purified, cleaned with Montage filter units (Millipore Corp.), and sequenced bidirectionally using the same primers, BigDye chemistry and an ABI 3100 sequencer (Applied Biosystems Inc.).

Population genetic analyses

Statistical analyses of allozymes were conducted with GENEPOP (version 3.3, Raymond & Rousset 1995). Population structure of mitochondrial data was examined with ARLEQUIN (version 2.001, Schneider *et al*. 2000) using the AMOVA method of Excoffier *et al*. (1994) and assuming Kimura 2-parameter distances among haplotypes. Hierarchical groupings correspond to dives, vent fields and ridge axes as defined in Table 1 and Fig. 1. We used the 4-gamete test (Hudson & Kaplan 1985) to test the infinite-sites model for mitochondrial haplotypes. A parsimony network of mitochondrial haplotypes was constructed with TCS (*c*. 1.18, Clement *et al*. 2000).

The isolation with migration (IM) program (Hey & Nielsen 2004) was used to assess dispersal across geographical boundaries. We examined a special case of asymmetric immigration model involving four demographic parameters (θ_1, θ_2, m_1, m_2) (Takahata & Slatkin 1990; Wakeley & Hey 1997; Nielsen & Wakeley 2001; Hey & Nielsen 2004). We omitted ancestral population size and time of population splitting from the final analysis, because posterior distributions for these parameters were flat and uninformative. Effective population size [$\theta_i = 4N_{e(i)}u$] was allowed to vary among populations. Although our estimates of demographic parameters were based on a mitochondrial locus, we report estimates that were scaled to be consistent with nuclear loci (a fourfold difference). Rescaling these estimates allows comparison with nuclear gene data. Markov chain Monte Carlo (MCMC) methods employed a two-step heating option with four parallel chains. Each chain was run for ~5.3×10^7 steps and sampled at 1000-step intervals, following a burn-in period of 500 000 steps. Each analysis was conducted multiple times to assess convergence of estimates. MCMC sample paths were examined by eye to determine how well the chain was mixing. We also used the CODA package in R (R Development Core Team 2005) to assess convergence according to Geweke's (1992) and Gelman & Rubin's (1992) diagnostic criteria.

Immigration estimates [$M_i = 2N_{e(i)}m_{ij}$] were rescaled to find posterior probability distributions for the effective number of immigrants in population *i*. After updating all parameters in each generation of the chain, we evaluated the expression $M_i = \theta_i m_i/2 = 2N_{e(i)}m_{ij}$. We used MCMC sampling to estimate probabilities that effective sizes or immigration rates are different between populations. We defined an indicator function for step *j* in the MCMC data set that takes a value of one if a hypothesis is true. For example,

$$I(j) = \begin{Bmatrix} 1 \text{ if } m_1 > m_2 \\ 0 \text{ if } m_1 < m_2 \end{Bmatrix}.$$

The mean of this indicator function over *s* samples is an estimate of the posterior probability of the hypothesis:

$$\Pr(m_1 > m_2 \mid X) = \frac{1}{S}\sum_{j=1}^{s} I(j),$$

where X represents the data. Prior probabilities of all hypotheses were 0.5 under our prior parameterization. Note that the posterior probability that the two parameters are equal must be zero [e.g. $\Pr(m_1 = m_2 \mid X) = (0)$], since the posterior distributions are probability distributions (i.e. their integral is equal to 1) and the parameters of interest are continuous. If migration rates between populations are roughly the same, then we expect $\Pr(m_1 > m_2 \mid X)$ to be in the neighbourhood of 0.5, but if migration is asymmetric, then $\Pr(m_1 > m_2 \mid X)$ will be far from 0.5. Posterior odds ratios were computed as $P/(1 - P)$, where P is the posterior probability of the hypothesis with the highest statistical support (i.e. $P > 0.5$).

With very large sample sizes, strong statistical support may exist for asymmetric population parameters, even if the differences are small in magnitude. Such small differences would be considered biologically insignificant. We monitor the quantities m_i/m_j, θ_i/θ_j and M_i/M_j to determine whether the differences between the parameter estimates are biologically significant. We report the posterior means of these quantities.

MIGRATE-N (Beerli & Felsentein 2001) was also used to estimate migration rates and effective population sizes for the mitochondrial data. A Bayesian MCMC approach was used to obtain parameter estimates, and the same statistical methodology described above was used to test hypotheses. The chain did not converge with five or more populations, so populations were grouped by ridge axis into four populations [GOR = (GOR, NES), JDF = (CLE, COA, MVL, END), AXI, EXP]. Axial seamount (AXI) was treated separately because it was significantly different from other Juan de Fuca populations. The results are included as Supplementary material (Tables S1 and S2), because they were not substantively different from the pooled IM analysis for two populations [South = (GOR, NES), North = (CLE, COA, AXI, MVL, END, EXP)]. MIGRATE-N analysis of the allozyme data produced flat posterior distributions, so we do not report these results.

Model adequacy

To assess whether models assumed for IM analysis were adequate, we generated posterior predictive distributions (PPD) of the test quantities from simulations (Gelman *et al*. 2004; pp. 157–190). Simulated data based on the model parameterized with COI data were compared to the observed mitochondrial and nuclear data to assess model adequacy. Goals of these analyses include determining whether the model can predict the mitochondrial data (internal model validation) and determining whether the model calibrated with COI could predict the degree of population structure observed for allozymes (external model validation). Values of observed summary statistics computed from each population were compared to the distribution of values generated by the simulated data. We used three test quantities to determine if the model was consistent with the COI data: π (Tajima 1983), the average number of pairwise differences among sequences; θ (Watterson 1975), estimated from the number of segregating sites; and Tajima's *D* (Tajima 1989). We used F_{ST} (Wright 1969) to determine if the model was consistent with the allozyme data.

We simulated data by first drawing demographic parameters from their joint posterior distribution, $P(\theta_1, \theta_2, m_1, m_2 \mid X)$, where X represents the observed data. In practice, we can sample from this distribution by drawing a line from the MCMC data set. Sampling in this manner preserves the correlational structure among parameters in the joint posterior distributions. We then rescaled the parameters to use as input in the MS program (Hudson 2002), which uses a standard coalescent algorithm (Hudson 1990) to generate genealogies. For diploid, biparentally inherited loci, MS defines the immigration parameters as $2M_i = \theta_i m_i = 4N_{e(i)}m_{ij}$ and the effective size/mutation parameters as θ_1 and $r^2 = \theta_2/\theta_1$, the effective size of population 2 relative to population 1. To generate data that are haploid and maternally inherited, we multiplied the parameters by the inheritance scalar, $h = 0.25$. Immigration parameters for MS become $M_i/2 = \theta_i m_i h = N_{ef(i)}m_{ij}$, and the effective size parameters become $\theta_1 h = N_{ef(1)}u$, where N_{ef} is the effective number of females in population 1, and $r^2 = \theta_2/\theta_1$. Note that we are making the assumption that the populations contain equal numbers of males and females when generating diploid, biparentally inherited parameters, since the model was parameterized using mitochondrial data. This assumption is justified by empirical observations: 1.08 female to male ratio (Urcuyo *et al*. 2003).

Using these rescaled parameters, we simulated genealogies with $2n$ tips for allozyme data and n tips for cytoplasmic data (see Table 1). Once we simulated a genealogy, we either randomly placed a single mutation on the genealogy to approximate diallelic allozyme loci or we placed mutations on the genealogy proportional to θ_1 to approximate our sequence data. We used this simulated data, X^{rep}, to compute the three summary statistics. We drew 5000 sets of parameters from their joint posterior distribution to estimate the PPD of the test statistics. These draws were widely spaced within the MCMC data set to reduce autocorrelation among the draws. In this manner, we generated posterior predictive distributions, $T_s(X^{rep}, \theta_1, \theta_2, m_1, m_2 \mid X)$, for each test statistic, s, conditional on the observed data, X.

It is important to note that the PPD determined by simulations are not estimates derived directly from the data, but are rather expectations derived from the model calibrated with the data. In this sense, the PPD represent expectations for the test quantities conditional on the model, where we have integrated across our uncertainty in the model parameters. If the model fits the data well, we expect the observed test quantities to fall somewhere near the centre of the posterior predictive distribution, but if the model does not fit the data well, one or more of the observed test quantities might fall in the tail of the posterior predictive distributions. Since our test quantities are sensitive to different aspects of the data (e.g. amount of total diversity or the frequency spectrum of mutations), the test statistics should be useful indicators of how the model is violated.

A convenient measure of the fit of the model is the posterior predictive *P* value, defined as the proportion of the predicted distribution for a particular test quantity that is more extreme than the observed test quantity. We compute *P* values describing how often summary statistics computed from the replicated data, X^{rep} are more extreme than those computed from the observed data, X:

$$p\text{S} = \Pr(T_S(X^{rep}, \theta_1, \theta_2, m_1, m_2) \geq T_S(X) \mid X).$$

Note that we did not condition on the genealogies in the MCMC data set.

Results

The circulation model

The circulation model estimated strong southeasterly flow around the Blanco Transform Fault (Fig. 1b). This pattern is consistent across depths ranging from 1500 to 3000 m. At 1500 m depth, a strong cyclonic current centred slightly east-northeast of the Cleft vent field (CLE) affects the summit of AXI and the southern Juan de Fuca Ridge. At 2000 m depth, stronger currents cross the southern Juan de Fuca Ridge near CLE and follow the Blanco Transform Fault towards the Gorda Ridge. Similarly, strong southeasterly currents were estimated at the approximate depth (3000 m) of the Gorda Ridge.

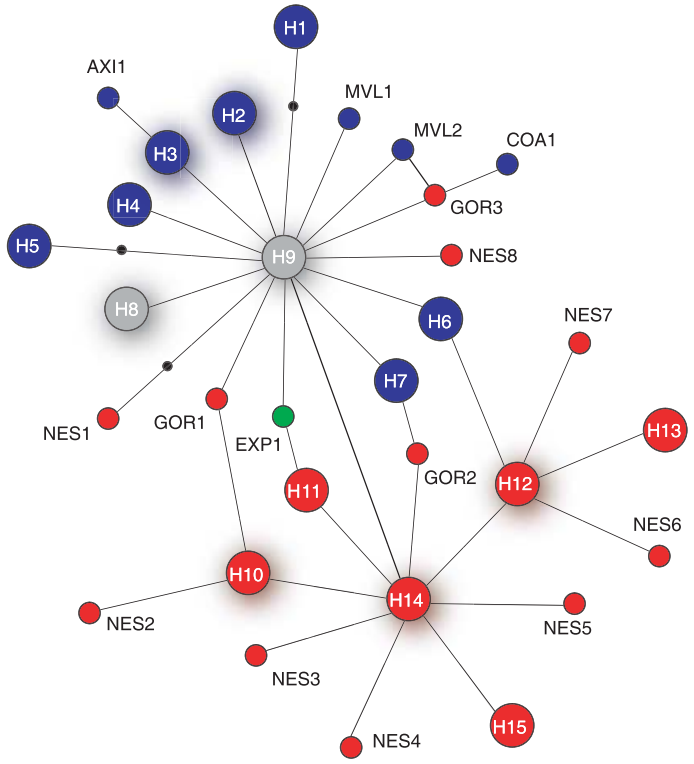

Hapl.	EXP	MVL	END	COA	AXI	CLE	GOR	NES	Total
EXP1	1								1
MVL2		1							1
MVL1		1							1
H1		1	1						2
H2	1	3		1					5
COA1				1					1
AXI1					1				1
H3					6	3			9
H4						2			2
H5						2			2
H6		1				1			2
H7		2	1			1			4
H8		1	6			3	1		11
H9	22	25	12	7	12	17	3	7	105
GOR1							1		1
GOR2							1		1
GOR3							1		1
H10							3	6	9
H11							1	2	3
H12							3	9	12
H13							1	3	4
H14							9	17	26
H15							2	2	4
NES1								1	1
NES2								1	1
NES3								1	1
NES4								1	1
NES5								1	1
NES6								1	1
NES7								1	1
NES8								1	1
n	24	35	20	9	19	29	26	54	216

Fig. 2 Parsimony network and geographical distribution of COI haplotypes. Blue haplotypes were observed north of the Blanco Transform Fault, and red haplotypes were observed south of the Blanco Transform Fault. Grey haplotypes were observed on either side of the Blanco Transform Fault. The green haplotype is from EXP across the Savanco Fracture Zone. Singleton haplotypes are represented as small circles and are named according to the vent field in which they were collected. Haplotypes observed more than once are labelled 'H', and haplotypes observed in five or more individuals are shadowed.

Population structure

We examined mitochondrial COI sequences (GenBank Accession nos: EU190494–EU190709) and four allozyme loci (Aat-1, Idh, Mdh-1, Mpi) (Table 1). A parsimony network of COI haplotypes (Fig. 2) resolves two overlapping groups, one of which is composed of haplotypes observed primarily south of the Blanco Transform Fault. COI diversity varied greatly among the population samples (range 0.16–0.93, mean = 0.64) and increased in the southerly direction (Fig. 3). Gorda Ridge populations had the highest mitochondrial diversity. Allozyme diversity was relatively low everywhere and fairly homogeneous among the localities (Table 2 and Fig. 3).

Hierarchical analyses of COI variance revealed significant population structure. Very small differences existed among multiple samples collected from vent fields (Table 1) (AMOVA: $\phi_{SC} = 0.010$; $P = 0.054$). These small among-samples differences justified pooling multiple samples from a vent field for the subsequent analyses. Highly significant differences existed among vent fields (AMOVA: $\phi_{CT} = 0.326$; $P < 0.001$). To test whether ridge offsets impede larval dispersal, we examined hierarchical structure among vent fields nested within ridge axes. Variance among vent fields within axes was small (AMOVA: $\phi_{SC} = 0.041$; $P < 0.001$) compared to the large component of variance among axes (AMOVA: $\phi_{CT} = 0.378$; $P < 0.024$). Allozymes revealed a comparable proportion of variance among vent fields within ridges ($F_{SC} = 0.052$; 95% CI 0.007–0.082), but curiously the variance among ridges also was small ($F_{CT} = 0.046$; 95% CI 0.003–0.076). We re-examine this seemingly inconsistent degree of population structure for nuclear and cytoplasmic markers (Model adequacy section).

To determine which populations contribute most to the previous AMOVA, we examined pairwise F_{ST}'s for COI. AXI housed the most divergent Juan de Fuca population (mean pairwise $F_{ST} = 0.171$; Table 3). No difference existed between the Gorda Ridge populations ($F_{ST} \approx 0$). The between-ridge component of variance between Explorer and Juan de Fuca ridge samples also was small (mean pairwise $F_{ST} = 0.049$; Table 3), and comparable to differentiation among Juan de Fuca populations. The Sovanco Fracture Zone, which separates the ridges, does not contribute significantly to the between-ridge component of variance. In contrast, the

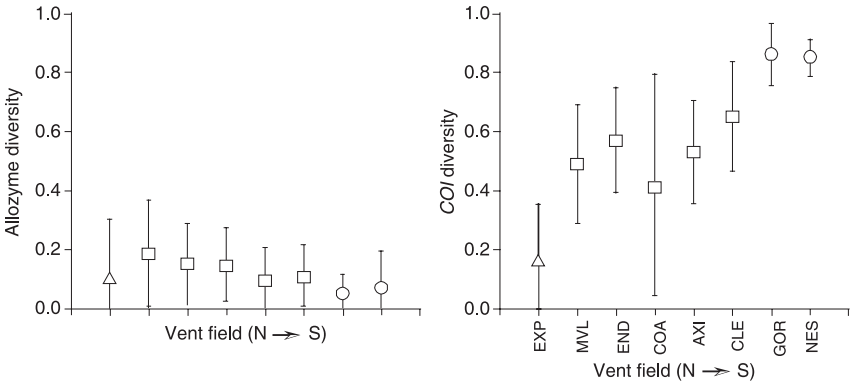

Fig. 3 Diversity estimates among vent fields for allozymes and COI. H_E, mean expected heterozygosity among allozyme loci; h, gene diversity of mitochondrial COI. Error bars are plus and minus 2 SE. Ridge axis indicators: triangles, Explorer Ridge; squares, Juan de Fuca Ridge; circles, Gorda Ridge.

Table 2 Allozymes: allelic frequencies and *F*-statistics

Locus/allele	EXP	MV	END	COAX	AXI	CLE	GOR	ET	F_{ST}	*P*
Aat-1 (*N*)	18	22	20	9	40	20	49	31	0.028	0.116
100	1.00	0.86	0.90	0.94	0.96	0.88	0.93	0.86		
80	—	0.14	0.10	0.06	0.04	0.13	0.07	0.15		
Idh (*N*)	18	22	20	9	40	20	49	31	0.023	0.220
100	1.00	1.00	1.00	1.00	1.00	0.98	1.00	1.00		
70	—	—	—	—	—	0.03	—	—		
Mdh-1 (*N*)	18	22	20	9	40	20	49	31	0.040	0.021
100	1.00	0.96	0.95	0.89	0.98	1.00	1.00	1.00		
70	—	0.05	0.05	0.11	0.03	—	—	—		
Mpi (*N*)	18	22	20	9	40	20	49	31	0.075	< 0.001
100	0.28	0.30	0.20	0.17	0.13	0.10	0.04	0.03		
90	0.72	0.71	0.80	0.83	0.85	0.90	0.96	0.97		
80	—	—	—	—	0.03	—	—	—		

Table 3 Proportion of mitochondrial diversity between populations. COI: Pairwise ϕ_{ST}, computed using K2P distances, is above diagonal and corresponding *P* value* is below diagonal. Allozymes: Pairwise F_{ST} is above diagonal and corresponding *P* value* is below diagonal. *P* values were computed by permutation

Marker	Vent field	EXP	MVL	END	COA	AXI	CLE	GOR	NES
COI	EXP	—	–0.012	0.155	0.028	0.266	0.025	0.425	0.411
	MVL	0.741	—	0.082	–0.019	0.183	0.024	0.399	0.409
	END	0.004	0.005	—	0.099	0.24	0.041	0.383	0.408
	COA	0.322	0.662	0.065	—	0.178	0.016	0.325	0.357
	AXI	**0.001**	**0.000**	**0.000**	0.025	—	0.082	0.417	0.425
	CLE	0.094	0.038	0.060	0.259	0.017	—	0.362	0.389
	GOR	**0.000**	**0.000**	**0.000**	**0.000**	**0.000**	**0.000**	—	–0.010
	NES	**0.000**	**0.000**	**0.000**	**0.000**	**0.000**	**0.000**	0.685	—
Allozymes	EXP	—	0.006	0.002	0.035	0.006	0.076	0.174	0.173
	MVL	0.273	—	–0.014	0.049	–0.007	0.040	0.145	0.110
	END	0.358	0.655	—	–0.001	–0.045	– 0.003	0.063	0.050
	COA	0.254	0.414	0.870	—	–0.013	0.002	0.065	0.061
	AXI	0.072	0.020	0.402	0.628	—	0.009	0.029	0.051
	CLE	0.028	0.063	0.407	0.172	0.384	—	0.008	–0.003
	GOR	**0.000**	**0.000**	0.007	0.016	0.050	0.242	—	0.010
	NES	**0.001**	**0.001**	0.026	0.003	0.061	0.398	0.189	—

*Bold type, significant at tablewide $\alpha = 0.05$ using sequential Bonferroni adjustment.

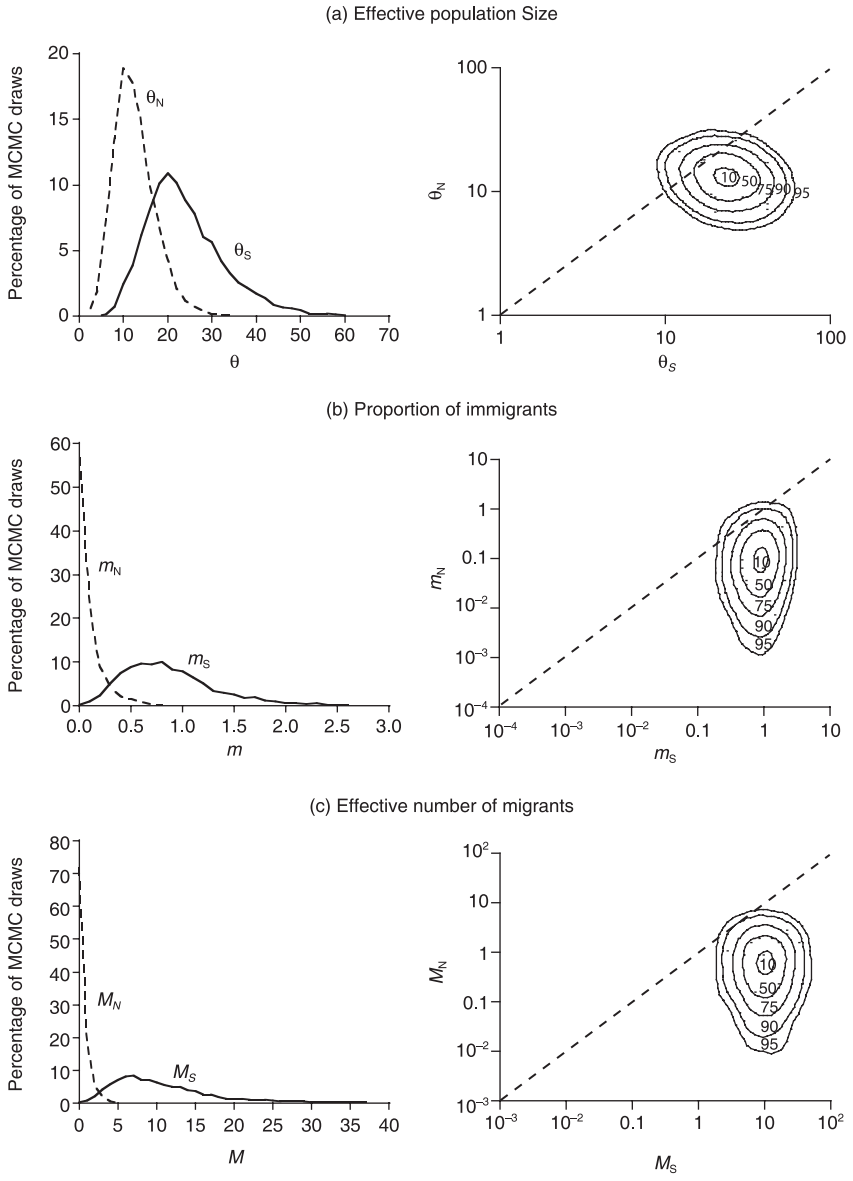

Fig. 4 (a) MPD and JPD of effective population sizes, θ_i. The dashed line in the right hand figure depicts equal effective population sizes for the northern and southern regions: $\theta_S = \theta_N$. The posterior probability that the effective population size of the southern region is greater than the effective population size of the northern region, $\Pr(\theta_S > \theta_N | X) = 0.87$, is the mass of this JPD below the dashed line. (b) MPD and JPD of the proportion of immigrants, m_i. The dashed line depicts equal proportions of immigrants in either population: $m_S = m_N$. $\Pr(m_S > m_N \mid X) = 0.98$. (c) MPD and JPD of the effective number of immigrants, M_i. The dashed line depicts equal numbers of migrants moving across the Blanco Transform Fault in either direction: $M_S = M_N$. $\Pr(M_S > M_N | X) = 0.99$.

Blanco Transform Fault is the dominant feature contributing to between-ridge population structure in *Ridgeia piscesae* (mean pairwise $F_{ST} = 0.392$). The pairwise F_{ST} estimates are correlated with two explanatory matrices (indicator of whether vent fields reside on the same ridge axis and the absolute difference in depth among sites). Although the two explanatory matrices are correlated (Mantel $r = 0.46$), partial correlations with F_{ST} estimates are significant for both factors (ridge axis: Mantel $r = 0.52$, $P = 0.049$; depth: Mantel $r = 0.68$, $P = 0.009$). Together these factors explain 62% of the variance in the pairwise F_{ST} matrix.

Estimation of demographic parameters

Based on mitochondrial population structure, *R. piscesae* could be partitioned into two groups separated by the Blanco Transform Fault. We used the IM program (Hey & Nielsen 2004) to investigate four demographic properties of these groups (Fig. 4). Population size, inferred from θ, was approximately twice as large in the southern group (Fig. 4a). The probability that $\theta_N > \theta_S$ equals 0.87 (similarly, from MIGRATE-N, $P = 0.85$), and the posterior-odds ratio is 7:1 in favour of the hypothesis that the Gorda Ridge vent fields have retained larger population sizes of these worms than northern vent fields along the Juan de Fuca and Explorer ridges.

Immigration was similarly biased. The proportion of immigrants in the southern group was about 11 times greater than those in the northern group (Fig. 4b). The probability that $m_S > m_N$ equals 0.98 (from MIGRATE-N, $P = 0.95$), and the posterior-odds ratio is 52:1 in favour of the hypothesis that the Gorda Ridge populations possess

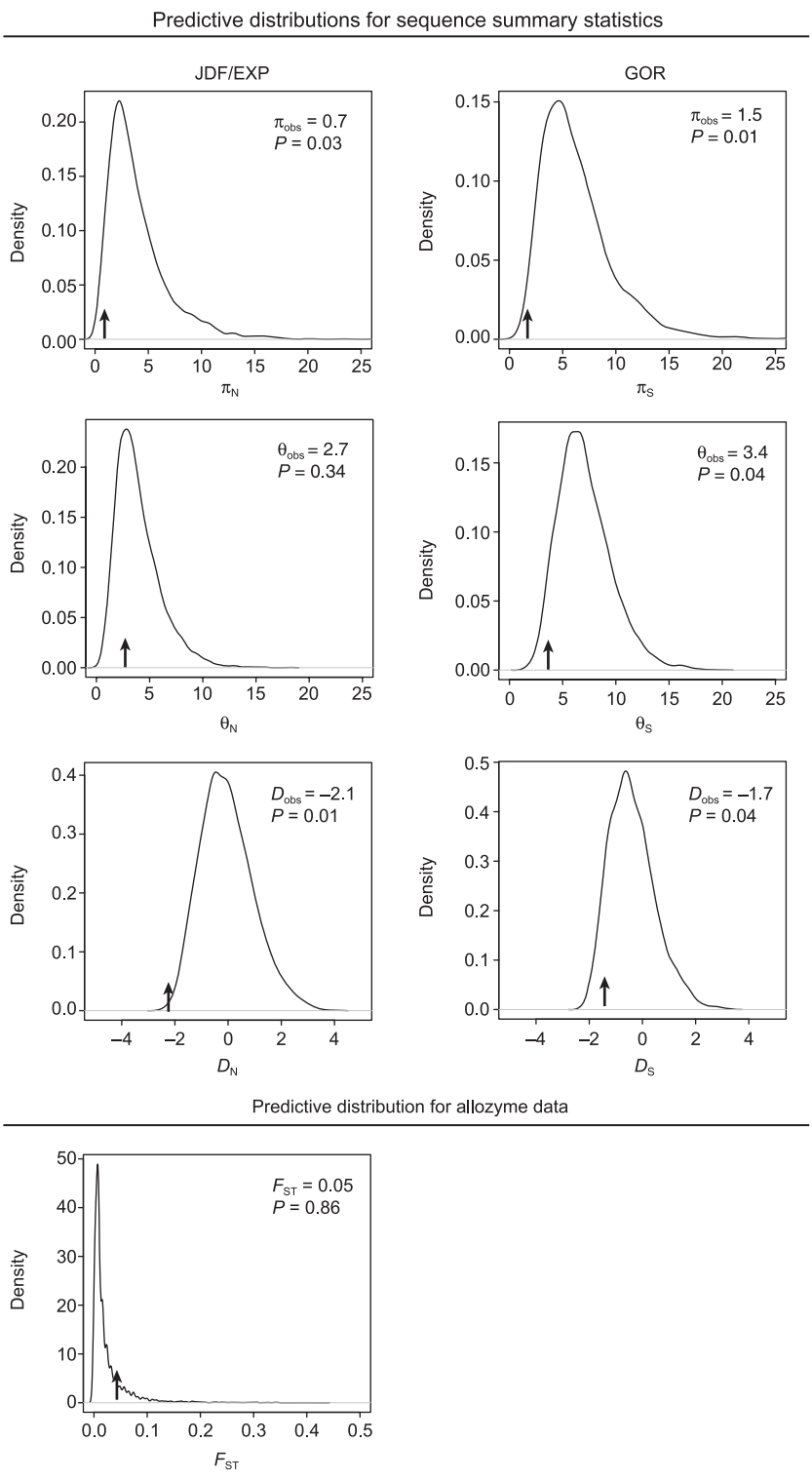

Fig. 5 PPD calculated from the island model calibrated with COI. Arrows and subscript 'obs' indicate observed values computed from the data. Summary statistics: π, theta estimated from the average number of pairwise differences; θ, Watterson's theta; *D*, Tajima's *D*; F_{ST}, Wright's F_{ST}. S, summary statistics computed from the southern population; N, summary statistics computed from northern population. *P* values are the proportion of the PPD that are more extreme than the observed value (see Methods for details).

more between-group immigrants than the northern populations. Rescaling these immigration rates by effective population sizes ($M_i = \theta_i m_i/2 = 2N_{e(i)}m_{ij}$) allows estimates of the effective numbers of immigrants per generation. Approximately 20 times more immigrants arrive in Gorda Ridge populations each generation (Fig. 4c). The probability that $M_S > M_N$ equals 0.99 (MIGRATE-N, $P = 0.97$), and the posterior-odds ratio is about 110:1 in favour of predominantly southward migration. According to present estimates, M_S is about 10 and M_N is less than one.

Our conclusions are robust to the population-pooling scheme as well as the complexity of the migration matrix assumed in parameter estimation. IM parameter estimates are similar if we only include GOR and CLE, populations that border the Blanco Transform Fault (Fig. S1, Supplementary material). These estimates are also completely consistent with estimates obtained from the four-population MIGRATE-N analysis (Fig. S2, Supplementary material) for migration across the Blanco Transform Fault (i.e. immigration into JDF and GOR). Other estimates of immigration between pairs of subpopulations within the northern group were not adequately resolved with the MIGRATE-N analysis. Nevertheless, immigration estimates for the Blanco Transform Fault region were insensitive to prior parameterizations of the poorly estimated parameters (prior sensitivity analysis, results not shown).

Model adequacy

We examined PPD to determine whether the COI data were plausible under the four-parameter demographic model that we assumed. Data were simulated from a demographic model, parameterized by the joint posterior distributions (JPDs, Fig. 4) generated by IM. The following test quantities were obtained from the simulations: π, the average number of pairwise differences among COI sequences; θ, the number of segregating sites in the sample; and Tajima's *D*. These quantities were estimated for each population separately (N, S). The 4-parameter model proved to be adequate in some respects, but not in others (Fig. 5). In general, the model predicts higher average pairwise differences (π) for both populations than the observed values, which likely results from an excess of rare mutations in the data compared to the model's predictions (e.g. Tajima's *D*, Fig. 5). Many demographic hypotheses exist that might explain the model's inadequacy: population growth on the timescale of the coalescent (Charlesworth *et al*. 1993; Tajima 1993); population subdivision (e.g. Wakeley & Aliacar 2001); or range expansion (Ray *et al*. 2003). However, an excess of rare mutations is common in data collected from hydrothermal vent taxa (Won *et al*. 2003; Hurtado *et al*. 2004; Johnson *et al*. 2006) and might also be the result of a high variance in reproductive success (Eldon & Wakeley 2006) among individuals found in these environments.

This simulation method also allowed us to examine an apparent discrepancy in population subdivision between the mitochondrial and allozyme markers. The fourfold difference in effective size of these marker systems might account for the difference in population structure. To determine whether the limited population structure observed for allozymes (F_{ST} = 0.046; 95% CI 0.003–0.076) is compatible with the predictions generated by the mitochondrial model, we simulated data by drawing parameters from the joint posterior distributions (Fig. 4), scaled fourfold to accommodate for nuclear loci. We randomly placed a new mutation on each genealogy to approximate a diallelic allozyme locus, and then computed Wright's F_{ST} (Wright 1969) for each simulated data set. The mean of the posterior predictive distribution for F_{ST} was 0.024 (95% probability interval: 0.0002–0.133; *P* value = 0.14), which is consistent with the observed value. Therefore, the degree of differentiation observed for allozymes agrees with expectations derived from the mitochondrial data (F_{ST}, Fig. 5).

Discussion

A deep-ocean circulation model generated in this study estimated strong southeasterly currents flowing along the Blanco Transform Fault. These predominant current vectors are expected to directionally bias the transport of passively dispersing marine larvae between the Juan de Fuca and Gorda ridge systems. Estimates of mitochondrial gene flow among populations of the vestimentiferan tubeworm *Ridgeia piscesae* were completely consistent with the predicted directional bias in larval transport. The effective number of migrants moving southward was estimated to be 20 times greater than those moving northward across Blanco Transform Fault. In contrast, the Sovanco Fracture Zone, a shorter ridge offset, does not similarly limit mitochondrial gene flow between the Juan de Fuca and Explorer ridges. Consequently, *R. piscesae* can be viewed as subdivided into northern and southern groups of populations separated by the Blanco Transform Fault. The mitochondrial data suggest that the southern populations from the Gorda Ridge sustain a larger metapopulation effective size.

A parallel pattern of geographical subdivision and demographic history occurs in *Lepetodrilus* limpets from this region. Johnson *et al*. (2006) partitioned what previously was considered a single species, *Lepetodrilus fucensis sensu lato*, into northern and southern sister species, *L. fucensis sensu stricto* and *L. gordensis* sp. nov., that are separated across the Blanco Transform Fault. If limited gene flow (introgression) occurs between the two species, analysis with the IM model revealed that it is similarly biased in a southward direction. Mitochondrial and nuclear sequence diversities also were markedly higher in the Gorda Ridge limpets, which is consistent with the pattern observed in *R. piscesae*. Nonetheless, the limpets and tubeworms differ in the degree of subdivision across the Blanco Transform Fault. This barrier played a historical role in isolating the limpet species vs. a contemporaneous role impeding the dispersal of the tubeworms. These temporal differences undoubtedly reflect unique aspects of their larval life histories and mechanisms of transport in the water column. Unfortunately, the life-history characteristics of all lepetodrilid limpets and most vestimentiferan tubeworms and are poorly known (Tyler & Young 1999; Marsh *et al*. 2001); nevertheless, dispersal abilities of these worms is thought

to be greater than that of the limpets, as indicated by previous studies of gene flow (Southward *et al*. 1996; Craddock *et al*. 1997; Vrijenhoek 1997). Despite these differences in dispersal potential, shared phylogeographical patterns suggest that common external factors have shaped their present-day population structure (*sensu* Avise 2000). Our results with *R. piscesae* are completely consistent therefore with the hypotheses put forth by Johnson *et al*. (2006): (i) that the Gorda Ridge has maintained historically larger populations of vent animals than the northern ridge systems; (ii) that the Gorda Ridge and Juan de Fuca/Explorer ridge systems form distinct dispersal corridors for vent-endemic taxa; (iii) that the Blanco Transform Fault has formed a historical isolating barrier for species with limited dispersal and an ongoing source of impedance for taxa with greater dispersal capabilities; and (iv) that dispersal of vent larvae across this barrier will be forced predominantly in a southerly direction. Additional evidence for these hypotheses is subsequently considered.

Allozymes did not exhibit identical degrees of population structure as mitochondrial COI in *R. piscesae*. This is a common result when examining evolutionary processes that act on very recent timescales, as has been reported for vent organisms that cross dispersal filters in the southeast Pacific and Atlantic oceans (Avise 2000; O'Mullan *et al*. 2001; Won *et al*. 2003). Our model adequacy analysis revealed that this apparent discrepancy is consistent with neutral divergence expected between nuclear and cytoplasmic markers with a fourfold difference in effective population size. In contrast, divergence between *Lepetodrilus fucensis and L. gordensis* estimated from allozymes and nuclear DNA sequences did co-vary with mitochondrial divergence, a likely consequence of the longer history of isolation between the limpet species (Johnson *et al*. 2006).

We find it noteworthy that overall patterns of mitochondrial diversity (θs) co-varied between the tubeworms and limpets. *Ridgeia piscesae* exhibited a step-cline in mitochondrial diversity that was highest in southern populations inhabiting the Gorda Ridge, intermediate along the Juan de Fuca Ridge, and lowest on the Explorer Ridge (Fig. 3). The step-cline might have resulted from a historical northward expansion of *R. piscesae* out of the Gorda Ridge region. Alternatively, effective population sizes of northern and southern populations might be different. Two lines of evidence refute the range expansion hypothesis. First, a parallel reduction in genetic diversity is not apparent in the nuclear loci examined in *R. piscesae* (Fig. 3). Second, *Lepetodrilus* limpets exhibit a similar pattern for mitochondrial COI, but divergence between the northern and southern limpets is likely to be millions of years old (Johnson *et al*. 2006). A recent range expansion cannot explain the difference in mitochondrial diversities of the northern and southern limpets. Thus, greater mitochondrial θs for the Gorda Ridge tubeworm and limpet populations is consistent with the hypothesis that the southern ridge axis sustains larger effective population sizes. Gorda Ridge vent fields are deeper (3200–3300 m) than the northern vent fields (1800–2400 m), and they are closer to the continental margin, which leads to heavy sedimentation. We suspect that these sediments create a diffusive lens that stabilizes the flux of sulphide venting. The spatial and temporal frequency of tectonic activity also differs between these ridge systems, because spreading rates increase with magma supply and vertical inflation of the ridge axis (Buck *et al*. 1998, and references therein). Habitat turnover should increase with spreading rates, leading to more frequent local extinctions and recolonization events, which in turn should accelerate the loss of genetic diversity (Vrijenhoek 1997). The step-cline in mitochondrial diversity of *R. piscesae* is consistent with the expected frequency of tectonic activity in this region, but further studies are needed before we can understand how sedimentation, depth, spreading rates, and latitude might affect habitat turnover and the maintenance of genetic diversity. Nevertheless, if our hypothesis is true, other vent-endemic animals from this region should exhibit similar patterns of genetic diversity. A control for these studies would be to examine deep-sea taxa from parallel environments that do not depend on the chemosynthetic productivity of hydrothermal vents.

Southerly mean currents as well as the depth difference between the Juan de Fuca and Gorda Ridges likely contribute to low northward dispersal across the Blanco Transform Fault. However, *R. piscesae* larvae do traverse this 450-km barrier in a southerly direction. The larval duration of *R. piscesae* is unknown, but it may be similar to that of *Riftia pachyptilla*, ~38 days (Marsh *et al*. 2001). *Riftia* tubeworm larvae are expected to disperse about 100 km on average, given the predominant current vectors measured along the northern East Pacific Rise by Marsh *et al*. (2001). With a larval duration of 38 days, *R. piscesae* larvae would require an average current velocity of 14 cm/s to traverse 450 km in one generation, which seems unlikely although current velocities are generally higher (4–20 cm/s) than the East Pacific Rise (1–5 cm/s) (Tyler & Young 1999). Perhaps larval duration is greater than 38 days in *R. piscesae*. Estimates of larval duration for this species and direct measurements of currents in this region are warranted. It is also possible that occasional venting along the Blanco Transform Fault facilitates dispersal of tubeworms across this region. Hydrothermal deposits and ^{3}He/heat anomalies were observed in the East Blanco Depression (Fig. 1a), although no vent megafauna were found (Hein *et al*. 1999). Further exploration of the Blanco Transform Fault for evidence of active venting is needed.

The present study has demonstrated the value of ocean circulation models for predicting regions of restricted larval dispersal in deep ocean communities. Our results are consistent with the hypothesis that larval dispersal occurs

primarily along corridors formed by the ridge axes, but may be interrupted by bathymetric features of the ridge system (reviewed in Vrijenhoek 1997; Van Dover *et al*. 2002). Strong currents interact with these bathymetric features to remove larvae from the supply of propagules that disperse among extant vent fields and colonize nascent fields, but the magnitude of these effects on population subdivision will differ among taxa as a consequence of their unique life histories and dispersal modes (Won *et al*. 2003; Hurtado *et al*. 2004).

Acknowledgements

The authors would like to thank R. Lutz and V. Tunnicliffe for sample collections and G. Pogson, S. Goffredi, V. Tunnicliffe, W. Lavelle, J. Hey, J. Jones, and anonymous reviewers for comments that helped clarify the manuscript. We gratefully acknowledge the contributions of the captains and crews of the R/V Atlantis II and the R/V Western Flyer and the pilots of the DSV Alvin and ROV Tiburon. S.F. updated the current model and generated the current data. C.R.Y. collected and analysed the genetic data. R.C.V. and C.R.Y. designed the experiment and co-wrote the manuscript. Funding for this project was provided by the Monterey Bay Aquarium Research Institute (The David and Lucile Packard Foundation) and NSF grants (OCE9910799 and OCE0241613).

References

Avise JC (2000) *Phylogeography: The History and Formation of Species*. Harvard University Press, Cambridge, Massachusetts.

Barber PH, Palumbi SR, Erdmann MV, Kasim Moosa M (2000) A marine Wallace's line? *Nature*, **496**, 692–693.

Beerli P, Felsentein J (2001) Maximum likelihood estimation of a migration matrix and effective population sizes in *n* subpopulations by using a coalescent approach. *Proceedings of the National Academy of Sciences, USA*, **98**, 4563–4568.

Bright M, Giere O (2005) Microbial symbiosis in Annelida. *Symbiosis*, **38**, 1–45.

Buck W, Delaney P, Karson J, Lagabrielle Y (1998) *Faulting and Magmatism at Mid-Ocean Ridges*, *Geophysical Monograph 106*. American Geophysical Union, Washington, DC.

Cavanaugh C (1994) Microbial symbiosis: patterns of diversity in the marine environment. *American Zoologist*, **34**, 79–89.

Charlesworth B, Morgan MT, Charlesworth D (1993) The effect of deleterious mutations on neutral molecular variation. *Genetics*, **134**, 1289–1303.

Clement M, Posada D, Crandall KA (2000) TCS: a computer program to estimate gene genealogies. *Molecular Ecology*, **4**, 331–346.

Craddock C, Lutz RA, Vrijenhoek RC (1997) Patterns of dispersal and larval development of archaeogastropod limpets at hydrothermal vents in the eastern Pacific. *Journal of Experimental Marine Biology and Ecology*, **210**, 37–51.

Eldon B, Wakeley J (2006) Coalescent processes when the distribution of offspring number among individuals is highly skewed. *Genetics*, **172**, 2621–2633.

Etter RJ, Rex MA (1990) Population differentiation decreases with depth in deep-sea gastropods. *Deep Sea Research Part A. Oceanographic Research Papers*, **37**, 1251–1261.

Etter RJ, Rex MA, Chase MC, Quattro JM (1999) A genetic dimension to deep-sea biodiversity. *Deep Sea Research Part I: Oceanographic Research Papers*, 1095–1099.

Excoffier L, Smouse P, Quattro JM (1992) Analysis of molecular variance inferred from metric distances among DNA haplotypes: Application to human mitochondrial DNA restricted data. *Genetics*, **131**, 479–491.

Folmer O, Black M, Hoeh W, Lutz R, Vrijenhoek R (1994) DNA primers for amplification of mitochondrial cytochrome *c* oxidase subunit I from metazoan invertebrates. *Marine Molecular Biology and Biotechnology*, **3**, 294–299.

France SC, Kocher TD (1996) Geographic and bathymetric patterns of mitochondrial 16S rRNA sequence divergence among deep-sea amphipods, *Eurythenes gryllus*. *Marine Biology*, **126**, 633–643.

Fujio S, Imasato N (1991) Diagnostic calculation for circulation and water mass movement in the deep pacific. *Journal of Geophysical Research*, **96**, 759–774.

Gage JD, Tyler PA (1991) *Deep Sea Biology: A Natural History of Organisms at the Deep-Sea Floor*. Cambridge University Press, Cambridge, UK.

Gelman A, Rubin D (1992) Inference from iterative simulation using multiple sequences. *Statistical Science*, **7**, 457–511.

Gelman A, Carlin JB, Stenrn HS, Rubin DB (2004) *Bayesian Data Analysis*. Chapman & Hall, New York.

Geweke J (1992) Evaluating the accuracy of sampling-based approaches to calculating posterior moments. In: *Bayesian Statistics*, **4** (eds Bernado J, Berger J, Dawid A, Smith A). Clarendon Press, Oxford, UK.

Goffredi SK, Hurtado LA, Hallam S, Vrijenhoek RC (2003) Evolutionary relationships of deep-sea vent and seep clams (Mollusca: Vesicomyidae) of the '*pacifica/lepta*' species complex. *Marine Biology*, **142**, 311–320.

Haymon RM, Fornari DJ, Von Damm KL *et al*. (1993) Volcanic eruption of the mid-ocean ridge along the East Pacific Rise crest at 9°45–52'N: direct submersible observations of seafloor phenomena associated with an eruption event in April, 1991. *Earth and Planetary Science Letters*, **119**, 85–101.

Hebert PDN, Beaton M (1989) *Methodologies for Allozyme Analysis Using Cellulose Acetate Gels*. Helena Laboratories, Beaumont, Texas.

Hein JR, Koski RA, Embley RW, Reid J, Chang S-W (1999) Diffuse-flow hydrothermal field in an oceanic fracture zone setting, northeast Pacific: deposit composition. *Exploration and Mining Geology*, **8**, 299–322.

Hey J, Nielsen R (2004) Multilocus methods for estimating population sizes, migration rates and divergence time, with applications to the divergence of *Drosophila pseudoobscura* and *D. persimilis*. *Genetics*, **167**, 747–760.

Hudson RR (1990) Gene genealogies and the coalescent process. *Oxford Surveys in Evolutionary Biology*, **7**, 1–44.

Hudson RR (2002) Generating samples under a Wright-Fisher neutral model of genetic variation. *Bioinformatics*, **18**, 337–338.

Hudson RR, Kaplan NL (1985) Statistical properties of the number of recombination events in the history of a sample of DNA sequences. *Genetics*, **111**, 147–164.

Hurtado LA, Lutz RA, Vrijenhoek RC (2004) Distinct patterns of genetic differentiation among annelids of eastern Pacific hydrothermal vents. *Molecular Ecology*, **13**, 2603–2615.

Johnson SB, Young CR, Jones WJ, Warén A, Vrijenhoek RC (2006) Migration, isolation, and speciation of hydrothermal vent limpets (Gastropoda; Lepetodrilidae) across the Blanco Transform Fault. *Biological Bulletin*, **210**, 140–157.

Kim S, Mullineaux LS (1998) Distribution and near-bottom transport

of larvae and other plankton at hydrothermal vents. *Deep Sea Research Part II: Topical Studies in Oceanography*, **45**, 423–440.

Kim SL, Mullineaux LS, Helfrich KR (1994) Larval dispersal via entrainment into hydrothermal plumes. *Journal of Geophysical Research*, **99**, 12,655–12,612,665.

Levitus S (1982) Climatological Atlas of the World Ocean. NOAA Prof. Pap., No. 13, pp. 173. U.S. Government Printing Office, Washington, D.C.

Levitus S, Boyer TP (1994) World Ocean Atlas 1994, Temperature, NOAA Atlas NESDIS, vol. 4, Natl. Oceanic and Atmos. Admin., Silver Spring, MD.

Marsh AG, Mullineaux LS, Young CM, Manahan DT (2001) Larval dispersal potential of the tubeworm *Riftia pachyptila* at deep-sea hydrothermal vents. *Nature*, **411**, 77–80.

Mullineaux LS, France SC (1995) Dispersal mechanisms of deep-sea hydrothermal vent fauna. In: *Physical, Chemical, Biological and Geological Interactions Within Seafloor Hydrothermal Systems* (eds Humphris SE, Zierenberg RA, Mullineaux LS, Thomson RE), pp. 408–424. Geophysical monograph 91. American Geophysical Union, Washington, D.C.

Mullineaux LS, Wiebe PH, Baker ET (1991) Hydrothermal vent plumes: larval highways in the deep sea? *Oceanus*, **34**, 64–68.

Mullineaux LS, Mills SW, Sweetman AK *et al*. (2005) Vertical, lateral and temporal structure in larval distributions at hydrothermal vents. *Marine Ecology Progress Series*, **293**, 1–16.

Nielsen R, Wakeley J (2001) Distinguishing migration from isolation: a Markov chain Monte Carlo Approach. *Genetics*, **158**, 885–896.

O'Mullan GD, Maas PAY, Lutz RA, Vrijenhoek RC (2001) A hybrid zone between hydrothermal vent mussels (Bivalvia: Mytilidae) from the Mid-Atlantic Ridge. *Molecular Ecology*, **10**, 2819–2831.

Palumbi SR (1994) Genetic divergence, reproductive isolation, and marine speciation. *Annual Review of Ecology and Systematics*, **25**, 547–572.

R Development Core Team (2005) *R: A Language and Environment for Statistical Computing*. R Foundation for Statistical Computing, Vienna, Austria.

Ray N, Currat M, Excoffier L (2003) Intra-deme molecular diversity in spatially expanding populations. *Molecular Biology and Evolution*, **20**, 76–86.

Raymond M, Rousset F (1995) GENEPOP (ver. 1.2): population genetics software for exact tests and ecumenicism. *Journal of Heredity*, **86**, 248–249.

Reid JL (1986) On the total geostrophic circulation of the South Pacific Ocean: flow patterns, tracers and transports. *Progress in Oceanography*, **16**, 1–61.

Reid JL (1997) On the total geostrophic circulation of the South-Pacific ocean: flow patterns, tracers, and transports. *Progress in Oceanography*, **39**, 263–352.

Schneider S, Roessli D, Excoffier L (2000) *ARLEQUIN, a Software Package for Population Genetics Data Analysis*. Genetics and Biometry Laboratory, Department of Anthropology, University of Geneva, Geneva, Switzerland.

Shank TM, Fornari DJ, Von Damm KL *et al*. (1998) Temporal and spatial patterns of biological community development at nascent deep-sea hydrothermal vents (9°50′N East Pacific Rise). *Deep Sea Research Part II: Topical Studies in Oceanography*, **45**, 465–515.

Southward EC, Tunnicliffe V, Black M (1995) Revision of the species of *Ridgeia* from northeast Pacific hydrothermal vents, with a redescription of *Ridgeia piscesae* Jones (Pogonophora: Obturata = Vestimentifera). *Canadian Journal of Zoology*, **73**, 282–295.

Southward EC, Tunnicliffe V, Black MB, Dixon DR, Dixon LRJ (1996) Ocean-ridge segmentation and vent tubeworms (Vestimentifera) in the NE Pacific. In: *Tectonic, Magmatic, Hydrothermal and Biology Segmentation of Mid-Ocean Ridges* (eds MacLeod CJ, Tyler PA, Walker CL), pp. 211–224. The Geological Society, London, UK.

Tajima F (1983) Evolutionary relationships of DNA sequences in finite populations. *Genetics*, **105**, 437–460.

Tajima F (1989) Statistical method for testing the neutral mutation hypothesis by DNA polymorphism. *Genetics*, **123**, 585–595.

Tajima F (1993) Statistical analysis of DNA polymorphism. *Japanese Journal of Genetics*, **68**, 567–595.

Takahata N, Slatkin M (1990) Genealogy of neutral genes in two partially isolated populations. *Theoretical Population Biology*, **38**, 331–350.

Thomson RE, Mihály SF, Rabinovich AB *et al*. (2003) Constrained circulation at Endeavour ridge facilitates colonization by vent larvae. *Nature*, **24**, 545–549.

Thurnherr AM, Speer KG (2003) Boundary mixing and topographic blocking on the Mid-Atlantic Ridge. *Journal of Physical Oceanography*, **33**, 848–862.

Tyler PA, Young CM (1999) Reproduction and dispersal at vents and cold seeps. *Journal of the Marine Biological Association of the United Kingdom*, **79**, 193–208.

Urcuyoa IA, Massothc GJ, Julian D, Fisher CR (2003) Habitat, growth and physiological ecology of a basaltic community of Ridgeia piscesae from the Juan de Fuca Ridge. *Deep-Sea Research*, **I** (50), 763–780.

Van Dover CL, German CR, Speer KG, Parson LM, Vrijenhoek RC (2002) Evolution and biogeography of deep-sea vent and seep invertebrates. *Science*, **295**, 1253–1257.

Vrijenhoek RC (1997) Gene flow and genetic diversity in naturally fragmented metapopulations of deep-sea hydrothermal vent animals. *Journal of Heredity*, **88**, 285–293.

Wakeley J, Aliacar N (2001) Gene genealogies in a metapopulation. *Genetics*, **159**, 893–905.

Wakeley J, Hey J (1997) Estimating ancestral population parameters. *Genetics*, **145**, 847–855.

Warren BA (1981) Deep circulation of the world ocean. In: *Evolution of Physical Oceanography* (eds Warren BA, Wunsch C), pp. 6–41. MIT Press, Cambridge, Massachusetts.

Watterson GA (1975) On the number of segregating sites in genetical models without recombination. *Theoretical Population Biology*, **7**, 256–276.

Won Y, Young CR, Lutz RA, Vrijenhoek RC (2003) Dispersal barriers and isolation among deep-sea mussel populations (Mytilidae: *Bathymodiolus*) from eastern Pacific hydrothermal vents. *Molecular Ecology*, **12**, 169–184.

Wright S (1969) *The Theory of Gene Frequencies*. The University of Chicago Press, Chicago, Illinois.

Rob Young, Research Fellow at Harvard University, conducts his research on the molecular ecology and evolution of deep-sea organisms, statistical genetics, and ecological theory related to the management of natural populations. Shinzal Fujio, Associate Professor of the Ocean Research Institute, the University of Tokyo, investigates deep ocean circulation by a combination of numerical modeling and direct current measurements. Robert Vrijenhoek, Senior Scientist at the Monterey Bay Aquarium Research Institute, focuses his studies on the molecular ecology and evolution of marine and aquatic organisms.

Supplementary material

The following supplementary material is available for this article:

Fig. S1 Posterior distributions and PPD from IM analysis of the GOR and CLE populations. (A) Marginal posterior probability distributions (MPD) and joint posterior probability distributions (JPD) of effective population sizes, θ_i, the proportion of immigrants, m_i, and the effective number of immigrants, M_i, in population i. Effective population size was about three times greater in GOR (θ_{GOR}) than CLE (θ_{CLE}), $\Pr(\theta_S > \theta_N \mid X) = 0.92$, P.O.R. = 12:1. The proportion of immigrants in GOR (m_{GOR}) was six times greater than CLE (m_{CLE}), $\Pr(m_S > m_N \mid X) = 0.93$, P.O.R. = 14:1. More than 25 times more immigrants arrive in GOR than CLE each generation, $\Pr(M_S > M_N \mid X) = 0.97$, P.O.R. = 32:1. (B) PPD calculated from the island model calibrated with COI using only samples collected from the two populations that flank the Blanco Transform Fault (CLE, GOR). Arrows and subscript 'obs' indicate observed values computed from the data. Summary statistics: π, theta estimated from the average number of pairwise differences; θ, Watterson's theta; D, Tajima's D; F_{ST}, Wright's F_{ST}. S, summary statistics computed from GOR; N, summary statistics computed from CLE. P values are the proportion of the PPD that are more extreme than the observed value (see Methods for details).

Fig. S2 Posterior distributions from MIGRATE-N analysis. Posterior distributions on the diagonal are estimates of theta, whereas posterior distributions off the diagonal are estimates of immigration rates (m_{ij} is migration from population i into j forward in time). Blank boxes are parameters that were not estimated (i.e. constrained to be zero). Posterior distributions for demographic parameters estimated from the southern populations (GOR and JDF) were insensitive to the prior parameterizations ($\theta_{MAX} = 0.10$, $m_{MAX} = 15\,000$). Estimates of demographic parameters from the AXI and EXP populations were sensitive to the prior parameterizations, and should not be trusted since we have no prior information on these parameters. However, given the stability of the immigration estimates for different prior parameterizations in the Blanco Transform Fault region, we are confident that our inferences for these parameters are not greatly affected by the prior information contributing to estimates of the other demographic parameters.

Table S1 Summary statistics and Wright–Fisher model tests

Table S2 AMOVA tables*

This material is available as part of the online article from:
http://www.blackwell-synergy.com/doi/abs/10.1111/j.1365-294X.2007.03609.x
(This link will take you to the article abstract).

Please note: Blackwell Publishing are not responsible for the content or functionality of any supplementary materials supplied by the authors. Any queries (other than missing material) should be directed to the corresponding author for the article.